ADVANCEMENTS IN EARTH-FAULT LOCATION IN COMPENSATED MV-NETWORKS

Janne ALTONEN, Ari WAHLROOS
ABB Oy Distribution Automation – Finland
janne.altonen@fi.abb.com, ari.wahlroos@fi.abb.com

Matti PIRSKANEN
Savon Voima Oyj – Finland
matti.pirskanen@savonvoima.fi

ABSTRACT

This paper discusses the challenges and requirements with regard to locating earth faults in compensated MV-networks. The work is based on the analysis of a comprehensive set of disturbance recordings from actual field tests conducted in co-operation with some Finnish power utilities. The performance of a novel earth-fault location algorithm based on the fundamental frequency impedance is evaluated with simulated and field test data by taking into account practical uncertainties including primary measurement errors, line parameters and the fault resistance. The results show that solid earth faults can be located without strict requirements on the accuracy of measurements or line data. However, as the fault resistance increases, the requirements for quality of measurements and validity of line parameters become more demanding. The fault resistance estimate additionally given by the algorithm is therefore a key indicator that can be used to evaluate the validity of the fault distance estimate in practice.

INTRODUCTION

In recent years earth-fault location in high-impedance earthed networks using fundamental frequency phasors has been under research and development in order to find a practically applicable solution for fault distance estimation, e.g. see references [1-2].

This paper studies a novel fundamental frequency based solution for locating earth-faults in compensated networks, confirms its performance in practice and evaluates the key factors affecting it.

THEORY

In principle the concept presented in reference [1] for locating earth-faults in unearthed networks can also be applied in compensated networks. The whole load of the feeder is modelled into one equivalent load tap located at *equivalent load distance* from the substation. The value of this parameter can be found out by simple network calculations, which can easily be supported by the DMS. The algorithm is based on the symmetrical component network models of *Fig. 1* and *2*.

The following notations are used in *Fig. 1* and *2*:
d = Per unit fault distance (d = 0…1).
s = Per unit distance of the equivalent load tap (s = 0…1).
$\underline{Z}_1$ = Positive-sequence impedance of the protected feeder.

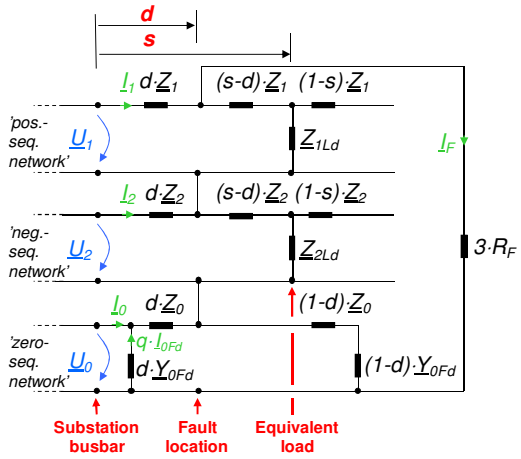

***Fig. 1**. Symmetrical component equivalent circuit for a single phase-to-earth fault located in front of the equivalent load tap.*

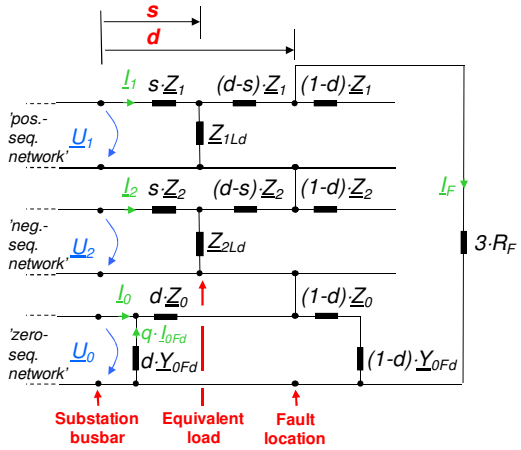

***Fig. 2**. Symmetrical component equivalent circuit for a single phase-to-earth fault located behind the equivalent load tap.*

$\underline{Z}_{1Ld}$ = Positive-sequence impedance of the load.
$\underline{Z}_2$ = Negative-sequence impedance of the protected feeder.
$\underline{Z}_{2Ld}$ = Negative-sequence impedance of the load.
$\underline{Z}_0$ = Zero sequence-impedance of the protected feeder.
$\underline{Y}_{0Fd}$ = Phase-to-earth admittance of the protected feeder per phase.
R_F = Fault resistance.
$\underline{I}_1$ = Positive-sequence current measured at IED location.
$\underline{I}_2$ = Negative-sequence current measured at IED location.
$\underline{I}_0$ = Zero-sequence current measured at IED location.
$\underline{I}_{0Fd}$ = Zero-sequence charging current of the feeder.
q = Distribution factor for zero-sequence current of the feeder.
$\underline{I}_F$ = Fault component current at fault point (actual fault current equals $3\cdot\underline{I}_F$).
$\underline{U}_1$ = Positive-sequence voltage measured at IED location.
$\underline{U}_2$ = Negative-sequence voltage measured at IED location.
$\underline{U}_0$ = Zero-sequence voltage measured at IED location.

Based on the equivalent circuit diagrams of *Fig. 1* and *2*, the following equations can be written. If the fault is located in front of the equivalent load tap ($d < s$), *Eq. 1* applies (refer to *Fig. 1*):

$$\Delta\underline{U}_0+\Delta\underline{U}_1+\Delta\underline{U}_2=d\cdot\underline{Z}_0\cdot(\Delta\underline{I}_0+q\cdot\Delta\underline{I}_{0Fd})+d\cdot\underline{Z}_1\cdot\Delta\underline{I}_1+\ldots \quad (1)$$
$$d\cdot\underline{Z}_2\cdot\Delta\underline{I}_2+3\cdot R_F\cdot\Delta\underline{I}_F$$

If the fault is located behind the equivalent load tap ($d \geq s$), *Eq. 2* applies (refer to *Fig. 2*):

$$\Delta\underline{U}_0+\Delta\underline{U}_1+\Delta\underline{U}_2=d\cdot\underline{Z}_0\cdot(\Delta\underline{I}_0+q\cdot\Delta\underline{I}_{0Fd})+s\cdot\underline{Z}_1\cdot\Delta\underline{I}_1+\ldots \quad (2)$$
$$(d-s)\cdot\underline{Z}_1\cdot\Delta\underline{I}_F+s\cdot\underline{Z}_2\cdot\Delta\underline{I}_2+(d-s)\cdot\underline{Z}_2\cdot\Delta\underline{I}_F+3\cdot R_F\cdot\Delta\underline{I}_F$$

In *Eq. 1* and *2*, the notation Δ ("delta") indicates a change in currents and voltages during the fault. In practice such a change can be accomplished by switching on or off the parallel resistor of the compensation coil during the fault.

The per unit fault distance d and the estimate for the fault resistance R_F in ohms can be obtained from *Eq. 1* and *2* by dividing them into real and imaginary parts. The logic for selecting between the results from *Eq. 1* and *2* is based on the calculated fault distance estimates: if d of *Eq. 1* is less than s, this is the valid fault distance estimate; otherwise the distance estimate is taken from *Eq. 2*.

The application of the concept "*equivalent load tap*" can be justified by the fact that the load of the feeder is under constant fluctuation, also during the change. On the other hand, the positive- and negative sequence admittances are neglected as the change does not affect the positive- and negative-sequence charging currents. In addition, the term $q\cdot\Delta\underline{I}_{0Fd}$ represents the part of the zero-sequence charging current component that is taken into account when calculating the voltage drop over the zero-sequence impedance $d\cdot\underline{Z}_0$.

One of the key input parameters of the algorithm is the total per phase phase-to-earth admittance of the protected feeder $\underline{Y}_{0Fd}$. It is used to estimate the change of the fault component current due to the parallel resistor switching (note that the actual fault current equals $3\cdot\underline{I}_F$):

$$\Delta\underline{I}_F=\Delta\underline{I}_0-\Delta\underline{U}_0\cdot\underline{Y}_{0Fd} \quad (3)$$

The parameter $\underline{Y}_{0Fd}$ can initially be given as a setting value based on DMS data, but it should be updated whenever the actual switching state of the feeder changes.

Other important input parameters are the zero- and positive-sequence impedances of the protected feeder (for lines applies $\underline{Z}_2=\underline{Z}_1$). In practice MV-feeders consist of multiple branches and conductor types and the impedance settings are typically selected according to the assumed main line of the feeder.

FIELD TESTING AND EXPERIENCE

Test arrangement

In order to illustrate the performance of the suggested earth-fault location algorithm, one trial earth-fault test series is studied. The tests were performed in a fully compensated 20 kV network owned by Savon Voima Verkko Oy, Finland. The disturbance recordings were captured at the substation with an oscilloscope in order to minimize the hardware related errors in the analysis. The configuration of the test feeder and the three fault locations (F.L. #1, #2 and #3) are shown in *Fig. 3*. Both solid and low-ohmic faults using a 500 Ω artificial fault resistor were conducted in all fault locations. The change during the earth-fault was accomplished by connecting a 4 A (at 20 kV) resistor in parallel with the compensation coil.

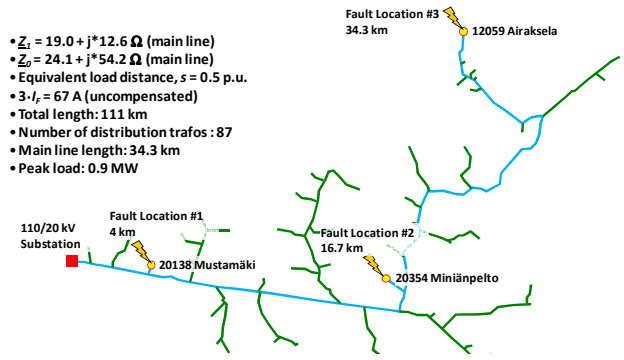

***Fig. 3**. Test feeder configuration. The main line is marked with blue colour.*

The line parameters of the test feeder were measured from the substation to the fault locations #2 and #3 in order to validate the initial line data based on the DMS. To enable such a measurement the feeder was taken out of use for a short period. As the measured zero-sequence resistance value is affected by the earthing resistance of the fault locations, it was afterwards corrected according to the theoretical relation between the positive- and zero-sequence resistances valid for overhead lines. For the fault location #1 the impedances were obtained from DMS data. *Table 1* shows the final impedances from the substation to the fault locations.

***Table 1**. Impedance settings based on measurements (#2 and #3) and on DMS data (#1).*

F.L.	d (km)	d[4] (p.u.)	$\underline{Z}_1$ (Ω)	$\underline{Z}_0$ (Ω)	$\underline{Z}_0$, corrected[3] (Ω)
#3 [1]	34.3	1.00	19.0+j·12.6	7.5+j·54.2	24.1+j·54.2
#2 [1]	16.7	0.52	9.1+j·6.2	7.7+j·29.4	11.5+j·29.4
#1 [2]	4.0	0.12	1.5+j·1.5	2.1+j·7.0	N/A

[1] Based on primary impedance measurement, [2] Based on DMS data
[3] For overhead lines the relation $R_0 = (R_1+0.148)$ Ω/km was used
[4] Per unit fault distance is based on the loop reactance setting selected according to F.L. #3 ($X_{LOOP} = (2\cdot X_1+X_0)/3 = 26.5$ Ω)

Fig. 4 shows the apparent loop impedance diagram of the test feeder and the corresponding target fault distance values of the fault locations (marked with red dots). This diagram is drawn using DMS data and impedance measurement results. The non-homogeneity of the line impedance due to different conductor types of the main line can be clearly seen.

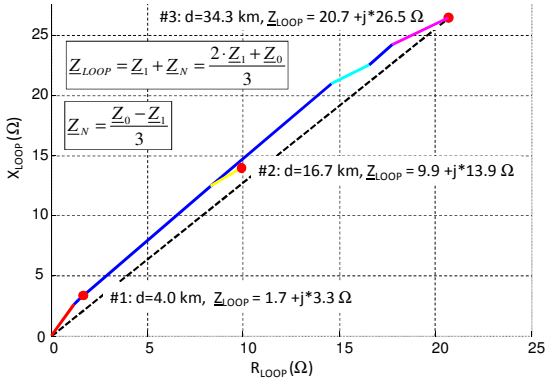

***Fig. 4**. Apparent loop impedance diagram of the main line of the test feeder. Each conductor type is marked with different colour.*

In order to study the effect of the voltage measurement accuracy when low amplitude phase-to-earth voltages are measured, three different sets of VTs/sensors were used.

Furthermore, the errors of the sensor voltage signals were compensated based on routine test report data valid down to 5% of U_n. For the VTs such data was not available. For the phase current measurement only one set of CTs was used, but the accuracy of these CTs was measured at site in order to enable error compensation. *Table 2* shows the basic data of the applied measurement transformers.

***Table 2**. Basic data of the measurement transformers used in the field tests.*

	type	class	notes
CT	KOFA 24D2	10P10	Existing CTs
VT #1	KRRS 20A1	0.5	Existing VTs, open-delta winding with ferroresonance damping resistor
VT #2	TJC 6	0.2	Installed for test, open-delta winding without ferroresonance damping resistor
Sensor	KEVCD AE3	1.0	Installed for test

The total per phase phase-to-earth admittance $\underline{Y}_{0Fd}$ of the test feeder was measured by conducting earth-fault tests outside the test feeder and then applying *Eq. 4*, in which the notation Δ now represents the change due to the fault.

$$\underline{Y}_{0Fd} = \Delta \underline{I}_0 / \Delta \underline{U}_0 \qquad (4)$$

The calculated $\underline{Y}_{0Fd}$ value varies slightly depending on the used measurement transformer combination as shown in *Table 3*. The resistive part of $\underline{Y}_{0Fd}$ is very small and its value is therefore more depending on the measurement accuracy.

***Table 3**. Results of the $\underline{Y}_{0Fd}$-measurements of the test feeder.*

	type	re($\underline{Y}_{0Fd}$) (mS)	im($\underline{Y}_{0Fd}$) (mS)	ratio im($\underline{Y}_{0Fd}$) / re($\underline{Y}_{0Fd}$)
#1	KRRS 20A1	0.00177	0.198	112
#2	TJC 6	0.00155	0.196	126
#3	KEVCD AE3	0.00235	0.197	84

Performance evaluation

Table 4 shows the result of the fault distance and fault resistance estimate calculations utilizing *Eq. 1-2*. They are based on the error compensated current and voltage signals. Voltages from sensors were used due to the expected highest accuracy. For impedance settings the values valid for the main line of the feeder (F.L. #3) was applied.

***Table 4a**. Fault distance and fault resistance estimates for solid earth faults (no artificial fault resistor).*

F.L.	d (p.u.) [2] $R_F = 0\ \Omega$	error (p.u.) [2]	R_{F_EST} (Ω)	R_{LOOP_TOT}/X_{LOOP} [1]
#1	0.17	0.05	-0.5	0.7
#2	0.52	0.00	11	1.6
#3	1.02	0.02	39	2.2

***Table 4b**. Fault distance and fault resistance estimates for low-ohmic earth faults (500Ω artificial fault resistor).*

F.L.	d (p.u.) [2] $R_F = 500\ \Omega$	error (p.u.) [2]	R_{F_EST} (Ω)	R_{LOOP_TOT}/X_{LOOP} [1]
#1	0.07	-0.05	515	280
#2	0.43	-0.09	512	46
#3	0.94	-0.06	551	23

[1] Ratio between the total estimated loop resistance ($R_{LOOP\_TOT} = R_{LOOP} + R_{F\_EST}$) and the estimated loop reactance (X_{LOOP}), [2] Per unit fault distance is based on the loop reactance setting selected according to F.L. #3 ($X_{LOOP} = (2 \cdot X_1 + X_0)/3 = 26.5\ \Omega$)

From *Table 4* it can be seen that the largest error occurs in fault location #1 in case of a solid earth fault. This is due to the fact that the actual impedance angle for this fault location does not match the impedance angle of the applied setting, which is based on fault location #3, see *Fig. 4*.

In low-ohmic faults (500 Ω artificial fault resistor) an approximately 0.1 p.u. difference in the results by comparison with the solid faults was observed despite the fact that the correctness of all line parameters was verified by measurements and all known error sources were cancelled out. This is evidently due to the fact that when the reactance part is extracted from the dominantly resistive impedance loop, the sensitivity of the fundamental frequency based algorithms to the correct input parameters and measurement signals becomes exceptionally high - even a minor error results in a large error in the fault loop reactance, i.e. the distance estimation. On the other hand, a fairly accurate fault resistance estimation, which also includes the earthing resistance of the fault location, is possible. Therefore, this additional information should be utilized in fault location purposes. For example, the errors in the fault distance estimates, *Table 4b*, could be cancelled out using the obtained fault distance estimates and the corresponding fault resistance estimates. In *Fig. 5* such a correction factor is shown as a function of the estimated fault resistance, which was obtained by first combining the results from the field tests and then interpolating the missing data through computer simulations. For example, when the fault resistance estimate equals 500 Ω, the estimated fault distance can be corrected by adding the corresponding correction factor to it in order to eliminate the influence of the fault resistance. In principle, such factors have to be considered separately for each feeder.

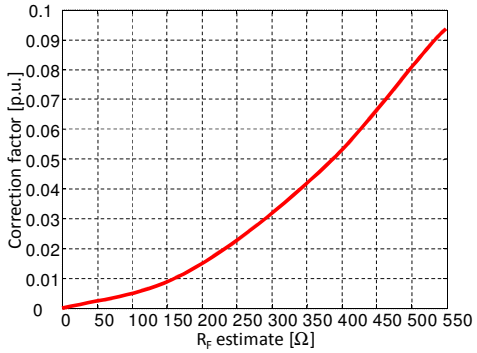

***Fig. 5**. Correction factor as a function of the estimated fault resistance.*

SENSITIVITY ANALYSIS

In the following a sensitivity analysis is performed regarding uncertainties existing in practice including fault resistance and errors in primary measurements and line parameters. The effect of the primary measurement accuracy on the fault distance estimation is shown in *Table 5*. It can be seen that the requirement for the quality of measurement highly depends on the actual fault resistance present at the fault location. Solid faults can be satisfactorily located with all measurement transformer combinations without any kind of error compensation. In case of a 500 Ω fault resistance, those measurement combinations where the voltages are measured with sensors provide meaningful results, even without error compensation. But if conventional VTs are used, phase and amplitude errors must be considered and cancelled out.

***Table 5a**. The sensitivity of the fault distance estimates with regard to accuracy of primary measurements, solid earth-faults (no artificial fault resistor).*

F.L.	d (p.u.) CT* & Sensors*	d (p.u.) CT & Sensors	d (p.u.) CT & VT #1	d (p.u.) CT & VT #2
#1	0.17	0.17	0.17	0.17
#2	0.52	0.52	0.51	0.52
#3	1.02	1.02	0.99	1.01

* with measurement error compensation

***Table 5b**. The sensitivity of fault distance estimate with regard to accuracy of primary measurements, low-ohmic earth-faults (500Ω artificial fault resistor).*

F.L.	d (p.u.) CT* & Sensors*	d (p.u.) CT & Sensors	d (p.u.) CT & VT #1	d (p.u.) CT & VT #2
#1	0.07	0.08	-0.19	-0.04
#2	0.43	0.46	0.19	0.36
#3	0.94	0.96	0.64	0.82

* with measurement error compensation

In *Fig. 6* the difference between the phase angles of phase-to-earth voltages measured by the sensor and the different VTs during a 500 Ω fault is illustrated, where the phase-to-earth voltage amplitude is 20% of its nominal value. It can be seen that in the worst case the phase angle difference reaches approximately 180 minutes (3 degrees), which largely explains the large error in the corresponding fault distance estimate, *Table 5b*. However, during the healthy state (with nominal voltage), the phase angle difference is only few minutes.

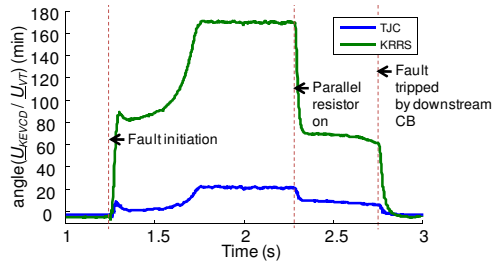

***Fig. 6**. The phase angle difference between the phase-to-earth voltages measured by the sensor and the VTs during a 500 Ω fault.*

The influence of the accuracy of the input parameter representing the total per phase phase-to-earth admittance $\underline{Y}_{0Fd}$ of the test feeder was found to be the most important. This is especially true, if the requirement for fault resistance coverage of a meaningful earth-fault location is extended from solid faults to low-ohmic faults. To illustrate this, results from the sensitivity analysis for $\underline{Y}_{0Fd}$ based on computer simulations is presented in *Fig. 7* – already an error of 5% is enough to make the validity of the fault distance to become poor at fault resistance values in the range of a few hundred ohms.

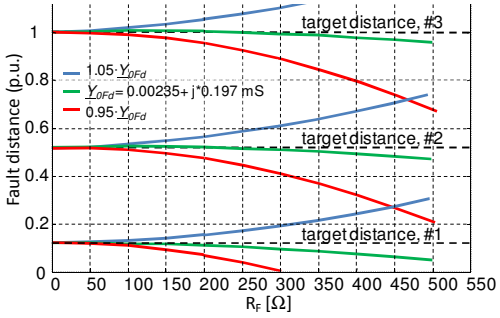

***Fig. 7**. Sensitivity of fault distance estimate with regard to the setting $\underline{Y}_{0Fd}$ as a function of the estimated fault resistance.*

The sensitivity of fault distance estimate with regard to the longitudinal line parameters given as settings is evaluated by studying the effect of possible amplitude and angle errors in setting $\underline{Z}_0$. This evaluation is justified as, in practice, especially the exact value of $\underline{Z}_0$ is typically unknown. The resulting errors in distance estimates are shown in *Table 6*. They are based on the error compensated current and sensor voltage signals. It can be concluded that the accuracy of the impedance settings directly affects the accuracy of the estimated fault loop reactance independently of the fault resistance.

***Table 6a**. The sensitivity of fault distance estimates with regard to deviations in $\underline{Z}_0$ setting, solid earth-faults (no artificial fault resistor).*

	Angle deviation in $\underline{Z}_0$		Amplitude deviation in $\underline{Z}_0$	
F.L.	error (p.u.) [1]	error (p.u.) [2]	error (p.u.) [3]	error (p.u.) [4]
#1	0.04	0.06	0.04	0.06
#2	-0.02	0.03	-0.03	0.04
#3	-0.02	0.08	-0.05	0.09

[1] +10 deg. deviation in angle($\underline{Z}_0$)
[2] -10 deg. deviation in angle($\underline{Z}_0$)
[3] +10% deviation in abs($\underline{Z}_0$)
[4] -10% deviation in abs($\underline{Z}_0$)

***Table 6b**. The sensitivity of fault distance estimates with regard to deviations in $\underline{Z}_0$ setting, low-ohmic earth-faults (500Ω artificial fault resistor).*

	Angle deviation in $\underline{Z}_0$		Amplitude deviation in $\underline{Z}_0$	
F.L.	error (p.u.) [1]	error (p.u.) [2]	error (p.u.) [3]	error (p.u.) [4]
#1	-0.05	-0.05	-0.06	-0.05
#2	-0.09	-0.08	-0.12	-0.06
#3	-0.08	-0.02	-0.12	0.01

[1] +10 deg. deviation in angle($\underline{Z}_0$)
[2] -10 deg. deviation in angle($\underline{Z}_0$)
[3] +10% deviation in abs($\underline{Z}_0$)
[4] -10% deviation in abs($\underline{Z}_0$)

CONCLUSIONS

The performance of a novel fundamental frequency based solution for locating earth-faults in compensated networks was studied by a sensitivity analysis concerning the practical uncertainties of the key input parameters required by the method. The results show that the practical accuracy of the algorithm depends on the fault resistance and the quality of the measurement signals and input parameters. As the fault resistance increases, adequate quality of measurements and accuracy of line parameters are the key factors for the method to enable a meaningful earth-fault location. Despite the fact that the suggested algorithm utilizes changes in measured currents and voltages during the fault, the requirement for high measurement accuracy cannot be avoided. In addition, the fault resistance estimate given by the algorithm is a key indicator regarding the validity of the fault distance estimate in practice. However, solid earth-faults can be located without strict requirements on the said factors and DMS data can be directly utilized in selecting valid line parameter settings.

REFERENCES:

[1] J. Altonen, A. Wahlroos, "*Advancements in fundamental frequency impedance based earth-fault location in unearthed distribution networks*", CIRED 2007, Vienna

[2] S. Hänninen, M. Lehtonen, "*Earth fault distance computation with fundamental frequency signals based on measurements in substation supply bay*", VTT Research Notes 2153, Espoo 2002